Biosensors and Bioelectronics 34 (2012) 132–136

Contents lists available at SciVerse ScienceDirect

Biosensors and Bioelectronics

journal homepage: www.elsevier.com/locate/bios

Gold-coated silica-fiber hybrid materials for application in a novel hydrogen peroxide biosensor

Jianhua Shen, Xiaoling Yang*, Yihua Zhu*, Haigang Kang, Huimin Cao, Chunzhong Li

Key Laboratory for Ultrafine Materials of Ministry of Education, School of Materials Science and Engineering, East China University of Science and Technology, Shanghai 200237, China

ARTICLE INFO

Article history:
Received 6 December 2011
Received in revised form 21 January 2012
Accepted 24 January 2012
Available online 2 February 2012

Keywords:
K-gold solution
Gold-coated silica-fiber
Core–shell hybrid nanostructure
Biosensor
Horseradish peroxidase
Hydrogen peroxide

ABSTRACT

We describe the preparation and characterization of a novel type of core–shell hybrid material for application in a novel hydrogen peroxide biosensor, where the structure consists of a continuous gold shell that encapsulates the silica fiber. The SiO_2@Au nanofibers had been synthesized by electrospinning silica sol, and then golden seeds were *in situ* grown on the fiber, lastly the gold-seeded silica fibers were further coated by continuous gold shells. The above nanocomposites had satisfactory chemical stability, excellent biocompatibility and efficient electron transfer property, which may have potential application for the highly sensitive chemical or biological sensors. Cyclic voltammetry (CV) was used to evaluate the electrochemical performance of the SiO_2@Au nanocomposites at indium tin oxide (ITO). The biosensor showed high sensitivity and fast response upon the addition of H_2O_2 and the linear range to H_2O_2 was from 5×10^{-6} to 1.0×10^{-3} M with a detection limit of 2 μM (S/N = 3). The apparent Michaelis–Menten constant of the biosensor was 1.11 mmol L^{-1}. These results indicated that SiO_2@Au nanocomposites have potential for constructing of a variety of electrochemical biosensors.

© 2012 Elsevier B.V. All rights reserved.

1. Introduction

In the past several decades, Au nanoparticles (NPs) have attracted strong interest in the fundamental sciences. Due to its chemical and thermal stability, high biocompatibility, and very high electron transport capacity, Au NPs have been widely investigated for their potential uses in a range of technological and biological applications including potential uses such as photothermal therapies (Wijaya et al., 2009; Pissuwan et al., 2007), targeted labeling (Eck et al., 2008), surface-enhanced spectroscopies (Ni et al., 2008), biosensors (Li et al., 2005; Yan et al., 2008; Zhou et al., 2010), and chemical catalysis (Lee et al., 2011). However, the high surface energy of metal NPs with diameters in the low nanometer range often leads to aggregation (Zhao et al., 1998). To overcome this problem, Au NPs have been immobilized on solid supports, such as carbon (Shen et al., 2011), metal oxides (Donkova et al., 2011; Dotzauer et al., 2008), and silica (Zhu et al., 2011). Among which, silica/Au hybrid materials have been studied extensively in the last decade (Mulvaney et al., 2000; Gao and Koshizaki, 2011; Liaw et al., 2011). The technique of silica/metal hybrid NPs enhancing enzyme immobilization has become widely applied due to their high biocompatibility and conductivity (Yang and Zhu, 2007; Sun et al., 2007). However, the electrical contacting of redox enzymes with electrodes is apparently the fundamental pre-requisite for the development of bioelectronic systems (Yan et al., 2008). Therefore, attempting to decrease the electron transfer resistance between electrode surface and bioactive molecules is of first importance. One-dimensional fibrous structure has more advantages over the zero-dimensional spherical Au NPs in electron transfer due to their perfect network and high surface-to-volume ratio. They could facilitate electron transfer from the redox center of a protein, as a high volume molecule, to the electrode surface via the interconnected conductive paths of fibrous structure (Kang et al., 2010).

However, research into Au NPs-decorated silica fibers or core–shell hybrid is still very few at present. Wang et al. (2007) reported that gold nanoshells (consisting of a silica core and a thin gold shell) were self-assembled on the surface of 3-aminopropyltrimethoxysilane modified indium tin oxide (ITO) electrode. Our group has reported that mesostructured silica fibers synthesized by electrospinning silica sol could be used as templates for the *in situ* assembly of Au NPs, and the formation of continuous gold shells along the fiber axis via solution-phase reduction of an appropriate metal ion in polyvinylpyrrolidone solution (Kang et al., 2010). Unfortunately, the complicated method of solution-phase reduction is not conducive to industrial production. Hence, we meliorate the method to format gold shells along the fiber axis via formaldehyde reduction of the basic aqueous gold solution

* Corresponding authors. Fax: +86 21 64250624.
E-mail addresses: xlyang@ecust.edu.cn (X. Yang), yhzhu@ecust.edu.cn (Y. Zhu).

0956-5663/$ – see front matter © 2012 Elsevier B.V. All rights reserved.
doi:10.1016/j.bios.2012.01.031

(K-gold solution), and tailored the thickness and morphology of gold shell by the concentration ratio of the K-gold solution (Kuo et al., 2008; Gruber et al., 2010; Kim and Lee, 2008). Simultaneously, we systematically study the performance of the electrode and the immobilized horseradish peroxidase (HRP) onto the gold coating of SiO_2 fibers (SiO_2@Au-fibers).

Herein we introduced gold seeds onto fiber surface by *in situ* reduction of $AuCl_4^-$ on self-assembled polyelectrolyte (poly allylamine hydrochloride, PAH). This seed-mediated growth is further used to form continuous gold shells around the silica nanofibers. The integrity and thickness of the gold shell could be tailored by the concentration ratio of the K-gold solution. After immobilizing HRP onto the composite to construct a biohybrid system, the novel H_2O_2 biosensor could be used as a component for investigating bio-electrochemical activity. SiO_2@Au-fibers and HRP are co-immobilized into biocompatible polymer chitosan (CS), which possesses a number of attractive properties such as high permeability toward water, good adhesion, biocompatibility and good film formation, and then the mixture is modified on ITO to fabricate the working electrode (Zhou et al., 2010). Electrochemical measurements were conducted to investigate the catalytic performance of the proposed biosensor.

2. Experimental

2.1. Preparation of SiO_2@Au-fibers

SiO_2 fibers, the hard templates, were synthesized according to the method we reported previously (Kang et al., 2010). The SiO_2 fibers were coated with gold by the following two steps. Firstly, the gold seed particles were attached to the surfaces of SiO_2 fibers via the layer-by-layer (LBL) self-assembled method (Kang et al., 2010; Zhu et al., 2011). Subsequently, the complete gold shells were grown on the gold-seeded SiO_2 fibers cores in a variety of ways (Oldenburg et al., 1998; Pham et al., 2002). The K-gold solution was prepared by mixing K_2CO_3 and $HAuCl_4{\cdot}H_2O$ in ultrapure water. The solution changed from yellow to colorless within 40 min, and was stored in the refrigerator overnight without exposure to light before being used. The fibers carrying gold seeds were then added to the K-gold solution. The mixture was under ultrasonication for 10 min, and then the formaldehyde was added to reduce the K-gold solution. Depending upon the concentration ratio of the K-gold solution, the color of the solution changed from colorless to blue (or brown, green), indicating the different thicknesses of gold shells (see SI). Finally, the SiO_2@Au-fibers were washed three times by centrifugation and redispersion in ultrapure water.

2.2. Sensor fabrication

The ITO (resistivity < 15 Ω) was used as the substrate for electrode buildup and was cleaned by sonicating sequentially for 20 min each in acetone, 10% KOH in ethanol and ultrapure water. After the treatment, the different samples of SiO_2@Au-fibers were dispersed in 0.5% CS acetic acid solution with a few minutes of ultrasonication to achieve a 0.5 mg/mL concentration (SiO_2@Au-fibers-CS), respectively. After the pH of SiO_2@Au-fibers-CS was adjusted above 5 by using 1 M NaOH, the suspension was spin-coated onto the ITO (denoted as fibers1/ITO, fibers2/ITO, fibers3/ITO, fibers4/ITO, respectively, according to the coating concentration of $HAuCl_4$ on gold shell). Then 1 mL of SiO_2@Au-fibers4-CS and 0.25 mL of HRP solution (10 mg/mL, dissolved in 0.1 M PBS, pH 6.5) were mixed adequately. Finally, the mixture was spin-coated onto the ITO (SiO_2@Au-fibers4-CS-HRP/ITO). The modified ITO was dried and kept under dry condition at 4 °C.

2.3. Electrochemical measurements

Electrochemical measurements were carried out with a CHI 660C workstation (CH Instruments, Chenhua, Shanghai, China) connected to a personal computer. A three-electrode configuration was employed, consisting of an ITO serving as a working electrode, whereas Ag/AgCl (3 M KCl) and platinum wire served as the reference and counter electrodes, respectively. The area of an ITO electrode exposed to the solution was maintained at a constant 1.0 cm^2. All electrochemical experiments were carried out at room temperature and all experimental solutions were deaerated by nitrogen for at least 15 min, then a nitrogen atmosphere was kept during the whole electrochemical measurements.

3. Results and discussion

3.1. Characterization of SiO_2@Au-fibers

In this research, the hard template SiO_2 fibers play a key role in fabricating an excellent biohybrid system. The fibers are synthesized by electrospinning silica sol, and then the golden seeds were *in situ* grew on the fiber by LbL electrostatic self-assembly (Kang et al., 2010). The SiO_2 fibers presented apparently uniform diameter about 750 nm. And gold-seeded silica fibers showed the smooth surfaces of bare SiO_2 fibers, the surface of nanoparticle-decorated fibers look rough and there are many fine particles. The uniform distribution of biding sites created dense and homogeneous gold NPs ca. 4 nm, and the crystal lattice can be observed directly, with a spacing d of 0.24 nm, which corresponded to Au (1 1 1) (see SI). The gold-seeded silica fibers are further coated by continuous gold shells via formaldehyde reduction of the K-gold solution. SEM images show SiO_2@Au-fibers prepared by reducing K-gold solution (denoted as fibers1, fibers2, fibers3 and fibers4, according to $HAuCl_4$:SiO_2 (m/m) = 1; 2; 3; 4, respectively) (see SI). With the increase of $HAuCl_4$, more and more gold ions were reduced and absorbed on the surface of gold seeds formed at the self-assembled stage, and then gradually grew into larger particles to form continuous gold shell (Fig. 1). The TEM images indirectly verify that low concentration of the K-gold solution only results in small granules rather than larger nanograins, the possible reason of which is the structure of shell may be incomplete or defective.

For further illustrate the structure of the gold shell on the SiO_2 fibers, Fig. 1 shows representative TEM images of SiO_2@Au-fibers coated with different depths of gold shell. It can be seen that the average thickness of gold shell basically increases with the concentration of $HAuCl_4$. With continuous increasing in the concentration, more gold particles were absorbed onto the fiber surface and combined with each other to form complete shells. To verify the formation of gold shell, we employed X-ray diffraction (XRD, see SI) and measured the powder patterns before and after forming gold shell (A: SiO_2 fibers; B: SiO_2 fibers supporting gold seeds; C and D: SiO_2@Au-fibers with fibers2 and fibers4, respectively). The specific XRD patterns of pure gold, characterized by four peaks positioned at 2θ values of 38.2°, 44.4°, 64.7° and 77.7° which correspond to the (1 1 1), (2 0 0), (2 2 0) and (3 1 1) lattice planes of the cubic-phase Au, were not all present in the samples. The fibers carrying gold seeds only have a weak intensity peak at 2θ = 38.21° which is an index of (1 1 1) lattice planes, while for the core–shell fibers, all expected diffraction peaks for the face-centered cubic structure of gold are presented. And with the increasing of $HAuCl_4$, the XRD patterns

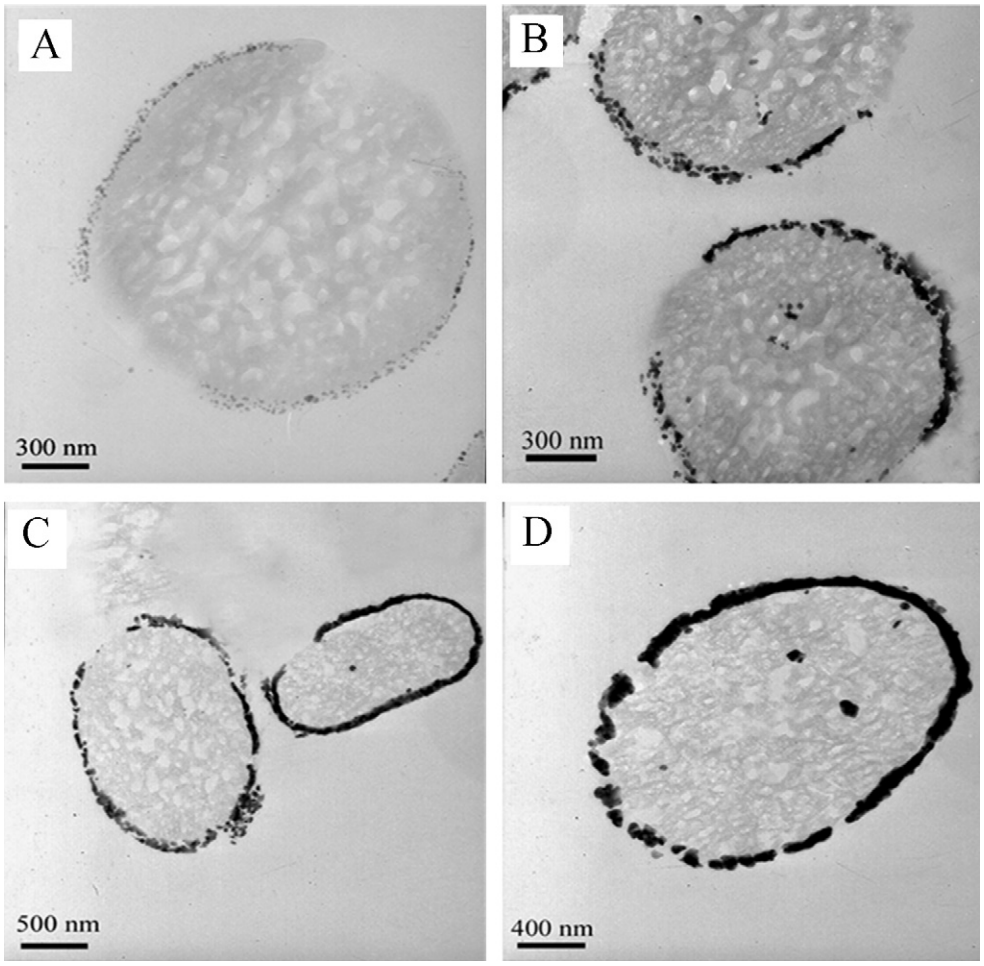

Fig. 1. Cross-section TEM images of SiO_2@Au core–shell fibers: (A) fibers1, (B) fibers2, (C) fibers3 and (D) fibers4, respectively.

of SiO_2@Au-fibers show strong diffraction peaks for the large gold NPs.

3.2. The electron transfer properties of SiO_2@Au-fibers-CS/ITO

Au NPs exhibit unique or improved electronic and optical properties. They can be easily modified using a wide range of biomolecules or chemical ligands and also facilitate electron transfer (Wang and Musameh, 2003), which make them one of the most promising materials to fabricate high performance biosensors. The impedance Nyquist plots spectra of the SiO_2@Au-fibers-CS/ITO are displayed in Fig. 2A. The data were recorded in the presence of 1 mM $Fe(CN)_6^{3-/4-}$ at $E = 0.2$ V (vs. SCE) with an ac potential modulation amplitude of 10 mV and for frequencies ranging between 100 mHz and 10 kHz. In these experiments $Fe(CN)_3^{3-/4-}$ was used as a redox label in solution, and the semicircle diameters lying on the *X*-axis of the plots are correspond to the interfacial electron transfer resistances at the electrode-solution interfaces. It is well established that the introduction of SiO_2@Au-fibers yields an electric layer on the electrode, resulting in a low electron transfer resistance (Kang et al., 2010). As compared to fibers4/ITO, the interfacial electron transfer resistance correspondingly decreased from ca. 230 Ω to ca. 100 Ω. The results indicate that the SiO_2@Au-fibers dramatically improved the ability of electronic transfer with the formation of the gold shell, because the electrons can be transported via the perfect network of the gold shell on the SiO_2 fibers.

Ferricyanide is always used as a probe to monitor the charge transport within the modified electrode. Fig. 2B shows the cyclic voltammograms (CV) of fibers1/ITO (a), fibers2/ITO (b), fibers3/ITO (c) and fibers4/ITO (d) in 5 mM $K_4Fe(CN)_6$ containing 1 mM KCl. A pair of redox peaks corresponding to the redox reaction of ferricyanide was observed. With the increase of the gold shell thickness, the peak currents both increased drastically while the peak-to-peak separation decreased. Further experimental data showed SiO_2@Au-fibers with the complete gold shell had better electron transport properties.

3.3. Electrochemical behaviors of the biosensor

The effect of the scan rate (v) on the peak currents (i_{pa} and i_{pc}) has been investigated in the range of 10–100 mV s^{-1}. Fig. 2C shows the CVs of the electrode denoted as SiO_2@Au-fibers4-CS-HRP/ITO at different scan rates in the potential range of −0.7 to +0.4 V in pH 6.5 PBS. As shown in the figure, the electrode displays prominent cathodic peak and anodic peak currents, suggesting that direct electron transfer was realized. And the peak currents and difference between peak potentials increased with the increasing of scan rate. The inset of Fig. 2C shows that the relationship between peak currents and the scan rates for the redox reaction of HRP are linear, indicating that the electrode process is a diffusionless system (Salimi and Ghadermazi, 2001). These findings suggest that the HRP has been successfully adsorbed onto the hybrid fiber surface.

The CVs of SiO_2@Au-fibers4-CS-HRP/ITO in different concentrations of H_2O_2 were also investigated. As shown in Fig. 2D, the cathodic peak current increased dramatically upon the addition of H_2O_2, which is a typical representation of the catalytic reduction

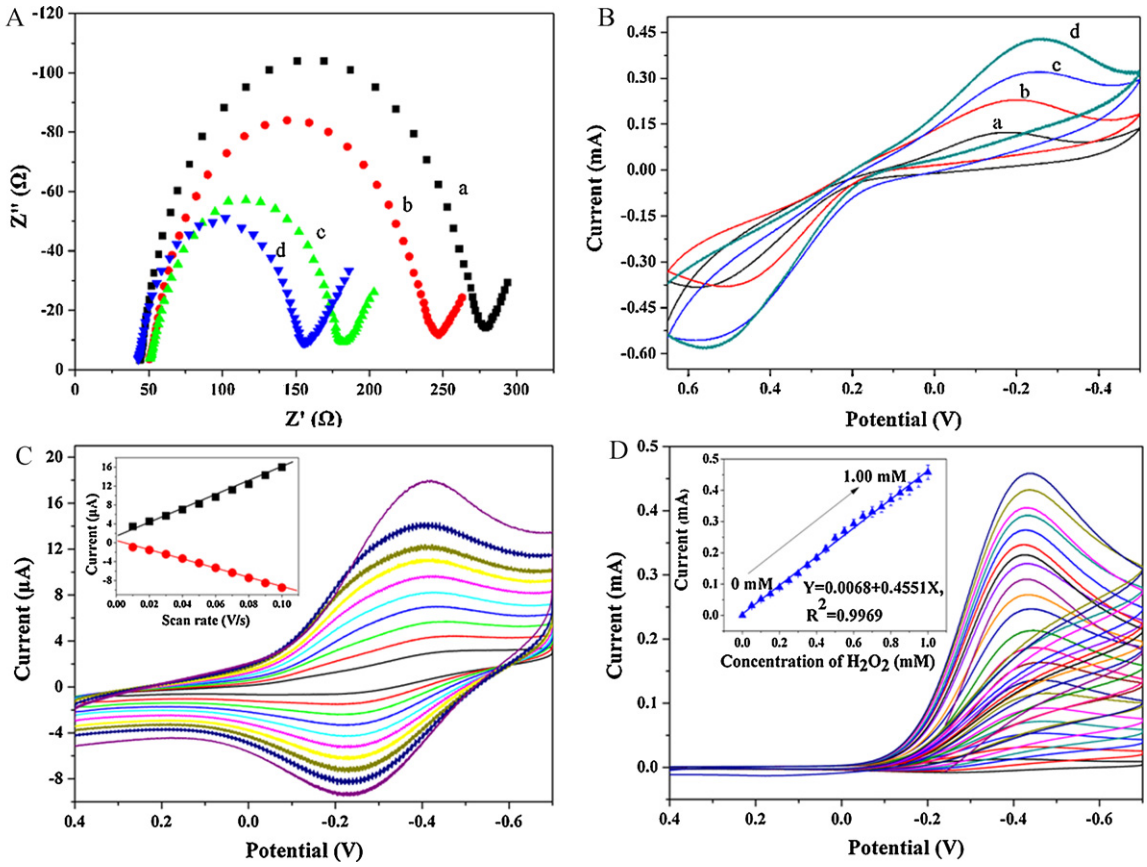

Fig. 2. (A) Faradaic-impedance spectra (Nyquist plots) of SiO_2@Au core–shell fibers. (B) Cyclic voltammograms of SiO_2@Au core–shell fibers in 5 mM $K_4Fe(CN)_6$ containing 1 mM KCl at a scan rate of 20 mV s^{-1}. (a) fibers1/ITO, (b) fibers2/ITO, (c) fibers3/ITO and (d) fibers4/ITO, respectively. (C) Cyclic voltammograms of SiO_2@Au-fibers4-CS-HRP/ITO in 0.1 M PBS buffer solution (pH 6.5) at different scan rates: 10, 20, 30, 40, 50, 60, 70, 80, 90 and 100 mV s^{-1}, respectively (from inner to outer). Inset: the relationship between peak currents and the scan rates for the redox reaction of HRP. (D) Cyclic voltammograms of SiO_2@Au-fibers4-CS-HRP/ITO with successive addition of 0.05 mM H_2O_2 at a scan rate of 0.1 V s^{-1}. Inset: the calibration curve of the amperometric response.

of H_2O_2. The catalytic mechanism of the immobilized HRP to H_2O_2 can be explained by the following scheme:

$$HRP(Fe^{3+}) + H_2O_2 \rightarrow \text{Compound I}(Fe^{4+}{=}O) + H_2O \quad (1)$$

$$\text{Compound I}(Fe^{4+}{=}O) + e^- + H^+ \rightarrow \text{Compound II} \quad (2)$$

$$\text{Compound II} + e^- + H^+ \rightarrow HRP(Fe^{3+}) + H_2O \quad (3)$$

HRP reacts with H_2O_2 to form a first intermediate (Compound I), which is a two-equivalent oxidized form containing an oxyferryl heme (Fe^{4+}=O) and a porphyrin π cation radical. Compound I shows the catalytic activity, and its porphyrin radical abstracts an electron from the electrode to form a second intermediate (Compound II), then Compound II is reduced back to the native HRP by accepting one electron from the electrode (Kafi et al., 2008). And the amperometric response of the electrode with successive injection of H_2O_2 was increased in Fig. 2D. The inset of Fig. 2D shows the calibration curve of the amperometric response. The biosensor has a good linear relationship with H_2O_2 to 1×10^{-3} M with a correlation coefficient of 0.997, which is similar to other hydrogen peroxide biosensors (Lei et al., 2004; Wang et al., 2009).

To further illustrate the steady-state amperometric response to H_2O_2 and the sensitivity of the proposed H_2O_2 biosensor, the typical current–time plot of the enzyme electrode resulted from successive injections of H_2O_2 was observed in the stirred buffer solution, as shown in Fig. 3. In the range between 0.4 and −0.7 V, the response increased first and then reached a pseudo-plateau for lower than −0.4 V, as shown in Fig. 2. Thus −0.4 V was selected as applied potential in subsequent experiments. When an aliquot of H_2O_2 was added into the stirring buffer solution, the reduction current rose sharply to reach a steady-state value. The biosensor responded rapidly when H_2O_2 was added and reached a steady state (95% of the maximum value) within 3 s, indicating a fast process and the immobilized HRP could well catalyze the reduction of H_2O_2. It is faster than the reported results of HRP that immobilized on AuNPs modified ITO electrode (≥5 s) (Wang et al., 2009; Zhao et al., 2002) and similar to that of HRP in AuNPs doped graphene electrode (Zhou et al., 2010). The faster response was mainly attributed to the follows: first, H_2O_2 can freely diffuse to the HRP molecules which are exposed to the surface of gold shell. Second, the SiO_2@Au-fibers with the complete network structure are favorable to the orientation of the HRP molecule and could provide a necessary conductive pathway to transfer electrons.

Fig. 3A shows the corresponding calibration plot of the biosensor. The currents had a good linear relationship with the concentration of H_2O_2 in the range of 5 μmol L^{-1} to 1.0 mmol L^{-1} with a correlation coefficient of 0.993. The biosensor has a detection limit of 2.0 μmol L^{-1} estimated at a signal to noise ratio of 3. The plot shows the corresponding Lineweaver–Burk curve while the concentration of H_2O_2 remains at a lower level. The apparent Michaelis–Menten constant (K_m), a reflection of both the enzymatic affinity and the ratio of microscopic kinetic constants (Kamin and Wilson, 1980), the K_m value for the SiO_2@Au-fibers-CS-HRP/ITO electrode was found to be 1.11 mmol L^{-1} (Fig. 3B). This result further shows that the biosensor exhibits higher biological affinity to H_2O_2 and the HRP enzyme on the gold shell kept its activity with a low-diffusion barrier.

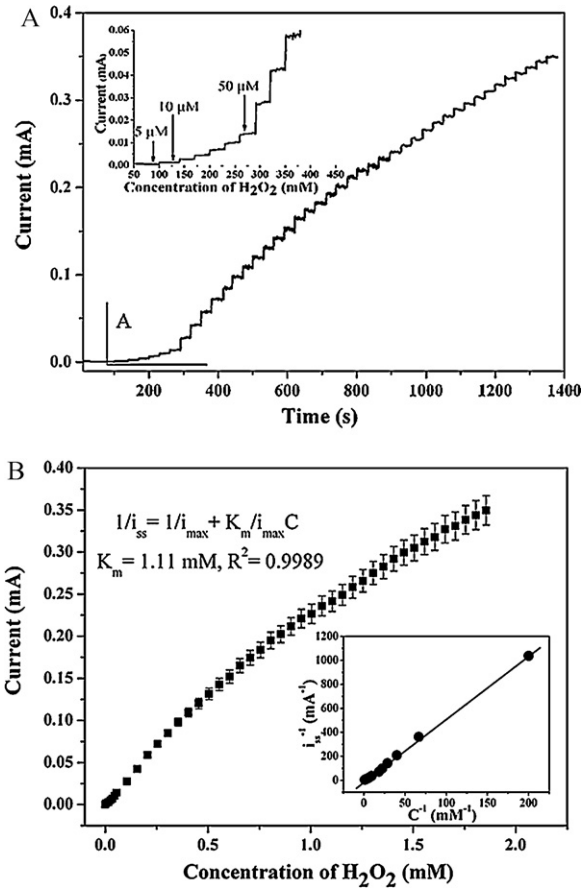

Fig. 3. (A) Current–time response of SiO_2@Au-fibers4-CS-HRP/ITO for successive addition of H_2O_2 in 0.1 M PBS (pH 6.5). Inset: amplification of part A. Operating potential: −0.4 V. (B) Calibration curve between the current and the concentration of H_2O_2. Inset: the corresponding Lineweaver–Burk plot.

The novel biosensor possessed good stability at 4 °C. The biosensor exhibited no obvious decrease in current response in the first week and maintained above 85% of its initial value after a month. The repeatability of the measurement was obtained by detecting 0.1 mM H_2O_2 10 times using the same electrode. And five electrodes were prepared utilizing the same method to check the reproducibility of the biosensor. Both of the relative standard deviations were found to be below 5%, which were acceptable.

4. Conclusions

To sum up, a novel hydrogen peroxide biosensor based on SiO_2@Au-fibers hybrid system has been presented. The SiO_2@Au-fibers have efficient electron transfer property and higher biological affinity, which may find potential application for the highly sensitive chemical or biological sensors. And the developed H_2O_2 biosensor had high sensitivity, wide linear range, low detection limit and good reproducibility. Furthermore, the promising platform presented here could be not only be used for fabrication of disposable biosensors based on HRP, it can be a promising option for the development of various oxidase-based biosensors and bioelectronic devices.

Acknowledgments

This work was supported by the National Natural Science Foundation of China (20925621, 20976054 and 21176083), the Special Projects for Nanotechnology of Shanghai (11nm0500800), the Fundamental Research Funds for the Central Universities, the Program for Changjiang Scholars and Innovative Research Team in University (IRT0825), and the Shanghai Leading Academic Discipline Project (project number: B502) for financial supports.

Appendix A. Supplementary data

Supplementary data associated with this article can be found, in the online version, at doi:10.1016/j.bios.2012.01.031.

References

Donkova, B., Vasileva, P., Nihtianova, D., Velichkova, N., Stefanov, P., Mehandjiev, D., 2011. J. Mater. Sci. 46, 7134–7143.
Dotzauer, D.M., Bhattacharjee, S., Wen, Y., Bruening, M.L., 2008. Langmuir 25, 1865–1871.
Eck, W., Craig, G., Sigdel, A., Ritter, G., Old, L.J., Tang, L., Brennan, M.F., Allen, P.J., Mason, M.D., 2008. ACS Nano 2, 2263–2272.
Gao, S., Koshizaki, N., 2011. Anal. Bioanal. Chem. 399, 91–101.
Gruber, S., Gottschlich, A., Scheel, H., Aresipathi, C., Bannat, I., Zollfrank, C., Wark, M., 2010. Phys. Stat. Sol. B 247, 2401–2411.
Kafi, A.K.M., Wu, G., Chen, A., 2008. Biosens. Bioelectron. 24, 566–571.
Kamin, R.A., Wilson, G.S., 1980. Anal. Chem. 52, 1198–1205.
Kang, H., Zhu, Y., Yang, X., Shen, J., Chen, C., Li, C., 2010. N. J. Chem. 34, 2166–2175.
Kim, J.H., Lee, T.R., 2008. J. Biomed. Pharm. Eng. 2, 29–35.
Kuo, W.S., Wu, C.M., Yang, Z.S., Chen, S.Y., Chen, C.Y., Huang, C.C., Li, W.M., Sun, C.K., Yeh, C.S., 2008. Chem. Commun., 4430–4432.
Lee, I., Joo, J.B., Yin, Y., Zaera, F., 2011. Angew. Chem. Int. Ed., doi:10.1002/anie.201007660.
Lei, C.X., Wang, H., Shen, G.L., Yu, R.Q., 2004. Electroanalytical 16, 736–740.
Li, C.Z., Male, K.B., Hrapovic, S., Luong, J.H.T., 2005. Chem. Commun., 3924–3926.
Liaw, J.W., Liu, C.L., Tu, W.M., Sun, C.S., 2011. J. Quant. Spectrosc. Radiat. Transfer 112, 893–900.
Mulvaney, P., Liz-Marzan, L.M., Giersig, M., Ung, T., 2000. J. Mater. Chem. 10, 1259–1270.
Ni, W., Yang, Z., Chen, H., Li, L., Wang, J., 2008. J. Am. Chem. Soc. 130, 6692–6693.
Oldenburg, S.J., Averitt, R.D., Westcott, S.L., Halas, N.J., 1998. Chem. Phys. Lett. 288, 243–247.
Pham, T., Jackson, J.B., Halas, N.J., Lee, T.R., 2002. Langmuir 18, 4915–4920.
Pissuwan, D., Valenzuela, S.M., Miller, C.M., Cortie, M.B., 2007. Nano Lett. 7, 3808–3812.
Salimi, A., Ghadermazi, M., 2001. Anal. Sci. 17, 1165–1170.
Shen, A., Guo, J., Xie, W., Sun, M., Richards, R., Hu, J., 2011. J. Raman Spectrosc. 42, 879–884.
Sun, Y., Yan, F., Yang, W., Zhao, S., Yang, W., Sun, C., 2007. Anal. Bioanal. Chem. 387, 1565–1572.
Wang, J., Musameh, M., 2003. Anal. Chem. 75, 2075–2079.
Wang, J., Wang, L., Di, J., Tu, Y., 2009. Talanta 77, 1454–1459.
Wang, Y., Qian, W., Tan, Y., Ding, S., Zhang, H., 2007. Talanta 72, 1134–1140.
Wijaya, A., Schaffer, S.B., Pallares, I.G., Hamad-Schicfferli, K., 2009. ACS Nano 3, 80–86.
Yan, Y.M., Tel-Vered, R., Yehezkeli, O., Cheglakov, Z., Willner, I., 2008. Adv. Mater. 20, 2365–2370.
Yang, H., Zhu, Y., 2007. Biosens. Bioelectron. 22, 2989–2993.
Zhao, M., Sun, L., Crooks, R.M., 1998. J. Am. Chem. Soc. 120, 4877–4878.
Zhao, Y.D., Zhang, W.D., Chen, H., Luo, Q.M., Li, S.F.Y., 2002. Sens. Actuators B: Chem. 87, 168–172.
Zhou, K., Zhu, Y., Yang, X., Luo, J., Li, C., Luan, S., 2010. Electrochem. Acta 55, 3055–3060.
Zhu, Y., Shen, J., Zhou, K., Chen, C., Yang, X., Li, C., 2011. J. Phys. Chem. C 115, 1614–1619.